Optimal Concentrations in Transport Systems

Kaare H. Jensen,[1] Wonjung Kim,[2,3] N. Michele Holbrook,[1] and John M. W. Bush[4,*]

[1]*Department of Organismic and Evolutionary Biology,*
Harvard University, Cambridge, MA 02138, USA
[2]*Department of Mechanical Engineering, Sogang University Seoul, Seoul 121-742, Republic of Korea*
[3]*Department of Mechanical Engineering, Massachusetts Institute of Technology, Cambridge, MA 02139, USA*
[4]*Department of Mathematics, Massachusetts Institute of Technology, Cambridge, MA 02139, USA*
(Dated: March 12, 2013)

Many biological and man-made systems rely on transport systems for the distribution of material, for example matter and energy. Material transfer in these systems is determined by the flow rate and the concentration of material. While the most concentrated solutions offer the greatest potential in terms of material transfer, impedance typically increases with concentration, thus making them the most difficult to transport. We develop a general framework for describing systems for which impedance increases with concentration, and consider material flow in four different natural systems: blood flow in vertebrates, sugar transport in vascular plants, and two modes of nectar drinking in birds and insects. The model provides a simple method for determining the optimum concentration c_{opt} in these systems. The model further suggests that the impedance at the optimum concentration μ_{opt} may be expressed in terms of the impedance of the pure ($c = 0$) carrier medium μ_0 as $\mu_{opt} \sim 2^\alpha \mu_0$, where the power α is prescribed by the specific flow constraints, for example, constant pressure for blood flow ($\alpha = 1$) or constant work rate for certain nectar drinking insects ($\alpha = 6$). Comparing the model predictions to experimental data from more than 100 animal and plant species, we find that the simple model rationalizes the observed concentrations and impedances. The model provides a universal framework for studying flows impeded by concentration, and provides insights into optimization in engineered systems, such as traffic flow.

I. INTRODUCTION

Transport systems are ubiquitous in nature and technology. Whether biological such as the vascular systems of plants and animals or engineered such as man-made pipes, roads, electrical grids, and the internet, they serve to move matter, energy, or information from one place to another. Due to the cost of constructing and maintaining redundant channels, it is advantageous for biological transport systems to distribute matter efficiently [1, 2]. Oxygen transport in vertebrates [3, 4], sugar transport in plants [5], and drinking strategies of many animals [6, 7] are known to be optimized for efficient transport of energy and material. Engineered systems must likewise be cost-effective and able to provide efficient transport under a variety of conditions; for example, considerable resources are spent annually to ease traffic congestion.

In our examination of transport systems, we consider material flow in four different natural systems: blood flow in vertebrates, sugar transport in vascular plants, and two modes of nectar drinking in birds and insects. A common feature of these and other transport systems is that the flow impedance depends on concentration. While the most concentrated solutions offer the greatest potential in terms of material transfer, the increase of impedance with concentration also makes them the most difficult to transport. Additionally, most transport systems are subject to a set of limiting constraints. For example, nectar feeders are typically constrained by a

constant work rate, which in turn is a function of flow impedance and hence concentration [7–9]. These transport systems may thus be characterized in terms of an optimization problem subject to appropriate constraints. This approach has been used to rationalize observed concentrations in a wide range of natural systems [4, 8–10]. For example, the observed volume fraction of erythrocytes (red blood cells), typical $\sim 40\% - 50\%$ in humans, has been shown to maximize oxygen transport [4, 10]. With the widespread use of bio-inspired design in the development of novel engineered systems, it seems likely that man-made transport systems such as roads or the electrical grid may benefit from improved understanding of natural transport systems.

We here develop a general framework for determining the concentration that maximizes material transfer in transport systems. By drawing on a number of natural examples – both new and derived from the biology literature – we show how these can be treated within a single framework that provides new insight into the efficiency of transport systems. We compare our model predictions to experimental data from more than 100 animal and plant species collected from the literature. Finally, we show that similar optimization criteria may be applied to engineered systems, and consider traffic flow in the context of our new framework.

II. GENERAL FORMULATION

We consider systems in which the material transfer rate (material flow) J can be expressed as the product of a

---

* Author for correspondence (bush@math.mit.edu)

volumetric flow rate (volume flow) Q and a concentration of material c

$$J = Qc \tag{1}$$

We express the volume flow as $Q = Xf/\mu$ where X is a constant geometric factor, f quantifies the mechanism driving the flow, and μ characterizes the impedance. The material flow in Eq. (1) can be expressed as

$$J = X\frac{f(c)}{\mu(c)}c \tag{2}$$

where f and μ can depend on c. We now seek the optimal concentration $c = c_{\text{opt}}$ that maximizes J in Eq. (2) subject to a set of constraints; constant driving force $f = f_0$ or constant work rate $W \sim Qf \sim f^2/\mu$. We therefore consider constraints of the form $f \sim \mu^\gamma$, where $\gamma = 0$ corresponds to constant driving force and $\gamma = 1/2$ to constant work rate when f depends on μ. Other values of γ are possible if there is a direct coupling between the driving force and impedance; for example, $\gamma = 5/6$ for bees that use viscous dipping to drink nectar (see Sec. III D).

Although we may have limited knowledge of the exact functional form of the concentration-dependent material flow $J(c)$ in Eq. (2), two general statements can be made. First, we expect J to be proportional to the concentration c at low concentrations and to approach zero with the concentration, i.e. $J(c) \propto c$ when $c \ll c_{\text{opt}}$. Second, we are concerned with situations where the system impedance increases with concentration, and J increases monotonically up to a maximum value $J(c_{\text{opt}})$. To describe the system, we therefore propose the first order governing equation

$$\frac{\partial J^*}{\partial c^*} = A - Bc^* \tag{3}$$

where $J^* = J(c)/J(c_{\text{opt}})$ and $c^* = c/c_{\text{opt}}$ is the normalized material flow and concentration, respectively. A and B are parameters which are determined by the boundary conditions: $J^*(0) = 0$, $J^*(1) = 1$, and $\partial J^*/\partial c^*|_{c^*=1} = 0$. This leads to

$$J^* = c^*(2 - c^*) \tag{4}$$

While Eq. (4) does not reveal the absolute value of the optimum concentration c_{opt}, it does contain information concerning the impedance at the optimum concentration $\mu(c_{\text{opt}})$. By expressing the constraint as $f \propto \mu^\gamma$, we find from Eq. (2) that the normalized flux $J^* = J(c)/J(c_{\text{opt}})$ can be written as

$$J^* = \frac{\mu(c)^\gamma}{\mu(c_{\text{opt}})^\gamma}\frac{\mu(c_{\text{opt}})}{\mu(c)}\frac{c}{c_{\text{opt}}} = \frac{c^*}{(\mu^*)^{1-\gamma}} \tag{5}$$

By using Eq. (4), the normalized impedance $\mu^* = \mu(c)/\mu(c_{\text{opt}})$ may be expressed as

$$\mu^* = \left(\frac{1}{2 - c^*}\right)^{1/(1-\gamma)} \tag{6}$$

It follows that the impedance at the optimum concentration is

$$\mu(c_{\text{opt}}) = 2^\alpha \mu(0) \tag{7}$$

where the power $\alpha = 1/(1 - \gamma) = \log_2(\mu(c_{\text{opt}})/\mu(0))$ and $\mu(0)$ is the impedance at zero concentration.

Eqns. (4), (6), and (7) provide a general framework for analyzing optimization of concentration impeded material flow in biological and engineered systems. To test the quantitative predictions of the theory we proceed in Sec. III by considering a series of biological examples where the flux J can be optimized along the lines outlined above. In Sec. IV, we apply our model to traffic flow. Finally, in Sec. V, we consider universal properties of concentration impeded material transport systems.

III.   BIOLOGICAL TRANSPORT SYSTEMS

A.   Nectar drinking from a tube

Perhaps the simplest situation in which we may apply Eq. (2) is drinking from a cylindrical tube. Many insects and birds such as butterflies and hummingbirds [7] feed on floral nectar, an aqueous solution of sugars, through tubes formed from probosci or tongues. Quick energy ingestion is advantageous for nectar feeders owing to the threat of predation. While the sweetest nectar offers the greatest energetic rewards, the increase of viscosity with sugar concentration also makes the sweetest nectar the most difficult to transport [14]. An optimal concentration may thus be sought for maximizing energy uptake rate.

Two different suction mechanisms are typically used by nectar feeders: active suction and capillary suction [7–9, 14]. Active suction feeders such as butterflies use muscle contraction to suck nectar through their roughly cylindrical probosci. In the limit of low Reynolds number Hagen-Poiseuille flow, the nectar mass flow rate J_s can be expressed as

$$J_s = \rho\bar{c}\frac{\pi a^4}{8\eta(\bar{c})l}\Delta p \tag{8}$$

where a is the radius and l the length of the proboscus, $\bar{c}$ is the wt/wt sugar concentration, η the viscosity (see Appendix A), ρ the density of the nectar solution, and Δp the pressure difference generated by muscular contraction. The manner in which biological constraints determined the dependence of the pressure Δp on nectar viscosity has been treated elsewhere [8, 9]. Active suction feeders are typically constrained by constant work rate $W = Q\Delta p = \pi a^4/(8\eta l)\Delta p^2$, so the pressure $\Delta p = (8Wl/(\pi a^4))^{1/2}\eta^{1/2}$ depends on viscosity and hence concentration. Comparing the nectar flow rate in Eq. (8) to the general expression in (2), we find that the impedance corresponds to the viscosity of the sugar solution $\mu = \eta$, the concentration to $c = \rho\bar{c}$, the geometric factor to $X = \pi a^4/(8l)$, and the driving mechanism to
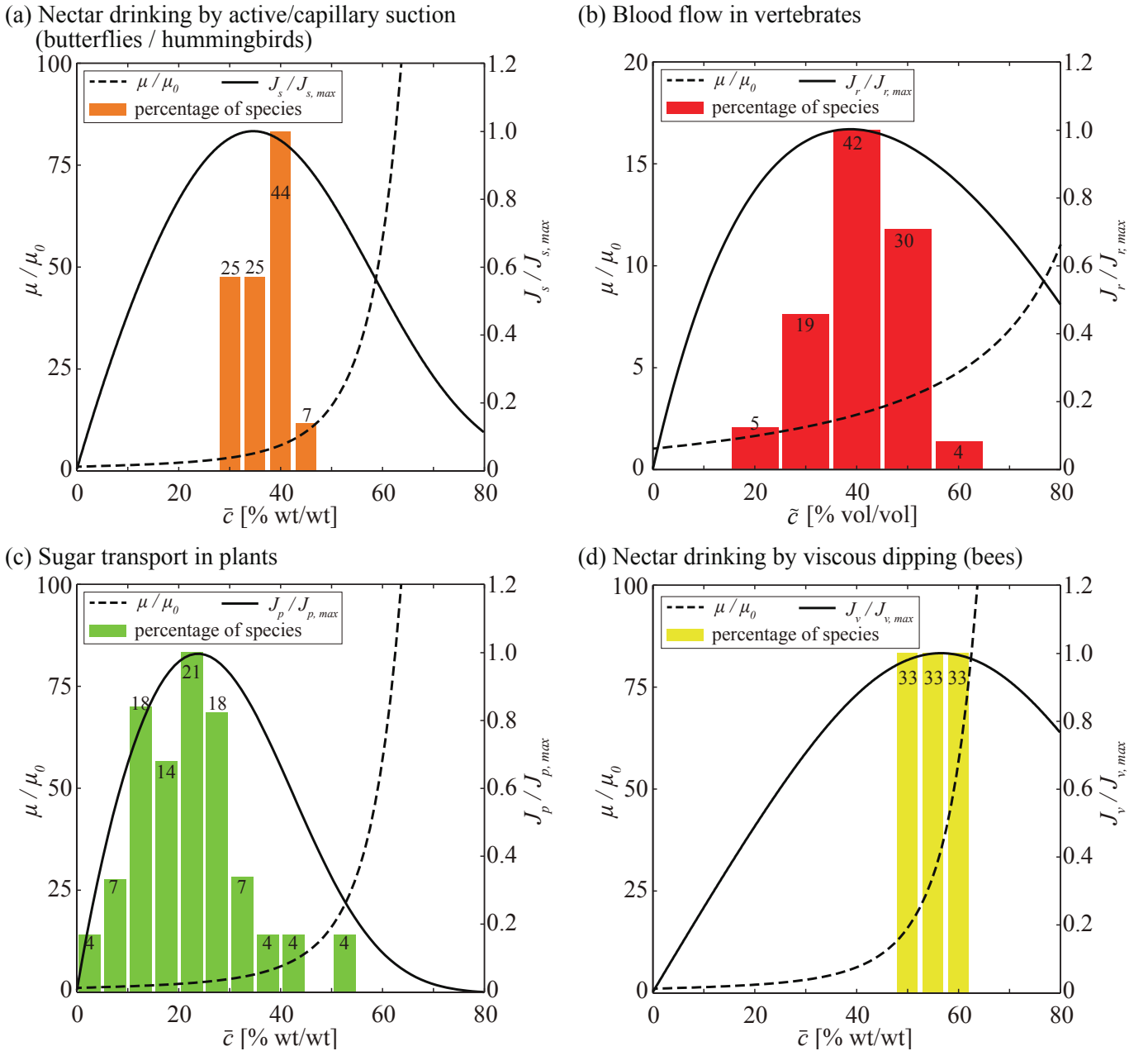
FIG. 1. Optimal concentrations in biological transport systems. (a) Drinking from a tube. Histogram showing distribution of observed sugar concentrations that maximizes nectar uptake for 16 bird and insect species that use muscular contractions or surface tension to feed through cylindrical tubes [9, 11]. Normalized sugar mass flow $J_s/J_{s,max}$ (solid line, Eqns. (8) and (9)) and nectar viscosity μ/μ_0 (dashed line, data from [12]) are plotted as a function of nectar sugar concentration $\bar{c}$. Mass flow is predicted to be maximum when $\bar{c}_{opt} = 35\%$, in good agreement with the observed average nectar concentration (37%). (b) Blood flow. Histogram showing distribution of observed red blood cell concentrations (hematocrit) from 57 vertebrate species [4]. Normalized oxygen flow $J_r/J_{r,max}$ (solid line, Eq. (10)) and blood viscosity μ/μ_0 (dashed line, see Appendix B) are plotted as a function of hematocrit $\tilde{c}$. Flow is predicted to be maximum when $\tilde{c}_{opt} = 39\%$, in good agreement with the observed average hematocrit (40%). (c) Sugar transport in plants. Histogram showing distribution of observed sugar concentrations from 28 plant species that use active sugar loading [13]. Normalized sugar flow $J_p/J_{p,max}$ (solid line, Eq. (11)) and sap viscosity μ/μ_0 (dashed line, data from [12]) are plotted as a function of phloem sugar concentration $\bar{c}$. Mass flow is predicted to be at a maximum when $\bar{c}_{opt} = 24\%$, in good agreement with the observed average sugar concentration (22%). (d) Nectar drinking by viscous dipping. Histogram showing distribution of observed sugar concentrations that maximizes nectar uptake for 6 insect species that use viscous dipping [9, 11]. Normalized sugar mass flow $J_v/J_{v,max}$ (solid line) and nectar viscosity μ/μ_0 (dashed line, data from [12]) are plotted as a function of nectar sugar concentration $\bar{c}$. Mass flow is predicted to be at a maximum when $\bar{c}_{opt} = 57\%$, in good agreement with the observed average nectar concentration (55%). In (a)-(d), the numbers given above the bins indicate the percentage of species in the bin. The experimental data are available in the Electronic Supplementary Material.

TABLE I. Parameters describing the material flow $J = Qc = Xfc/\mu$ (see Eq. (2)) for each of the systems considered. See Appendices A and B for details on the viscosity η of blood, nectar and phloem sap.

System	Geometry X	Driving force f	Concentration c	Impedance μ	Constraint
Nectar drinking (Active suction)	$\pi a^4 (8l)^{-1}$	Δp	$\rho \bar{c}$	η	Const. work rate $W = Q\Delta p$ $f \propto \mu^{1/2}$
Nectar drinking (Capillary suction)	πa^3	$(\sigma \eta T)^{1/2}(T+T_0)^{-1}(2a)^{-1/2}$	$\rho \bar{c}$	η	Cyclic suction period $T + T_0$ $f \propto \mu^{1/2}$
Blood flow in vertebrates	$\pi a^4 (8l)^{-1}$	Δp	$\tilde{c}$	η	Const. pressure $f_0 = \Delta p$ $f \propto \mu^0$
Sugar transport in plants	$\pi a^4 (8l)^{-1}$	Δp	$\rho \bar{c}$	η	Const. pressure $f_0 = \Delta p$ $f \propto \mu^0$
Nectar drinking (Viscous dipping)	$2\pi a^3$	$\eta u e a^{-2}$	$\rho \bar{c}$	η	Const. work rate $W = \eta u^2 l$ $f \propto \mu^{5/6}$
Traffic flow (Greenberg)	N	$\mathcal{C}$	ρ/ρ_m	$\ln(c_0/c)^{-1}$	Const. optimum speed $f_0 = \mathcal{C}$ $f \propto \mu^0$
Traffic flow (BHN)	N	v_{max}	ρ/ρ_m	$\tanh(\frac{1-\rho L}{\rho s})^{-1}$	Const. speed limit $f_0 = v_{\max}$ $f \propto \mu^0$

the pressure, $f = \Delta p$. We can thus express the constraint as $f = (8Wl/(\pi a^4))^{1/2}\mu^{1/2}$ (see Table I).

Capillary suction feeders such as hummingbirds use surface tension to draw nectar along their tongue, during repeated cycles of tongue insertion and retraction [7, 9]. If the duration of a cyclic motion is the sum of the nectar loading time T and unloading time T_0, the average nectar mass flow rate J_s can be expressed as $J_s = \rho \bar{c} \pi a^2 l(T)/(T + T_0)$ where $\pi a^2 l(T)$ is the time-dependent nectar volume extracted during the loading. In the loading phase the volumetric flow rate is given by $\pi a^2 (dl/dt) = \pi a^4 \Delta p/(8\eta l)$, where $\Delta p = 2\sigma/a$ is the capillary pressure. The solution with initial condition $l(0) = 0$ is given by $l(t) = (a\sigma t/(2\eta))^{1/2}$, which depends explicitly on viscosity and hence concentration. The average nectar mass flow rate J_s can be expressed as

$$J_s = \rho \bar{c} \frac{\pi a^3}{\eta(\bar{c})} \left(\frac{\sigma \eta(\bar{c})}{2a} \frac{T}{(T+T_0)^2} \right)^{1/2} \tag{9}$$

By comparing the nectar flow rate in Eq. (9) to the general expression in Eq. (2), we find that $X = \pi a^3$, $f = \left(\sigma \eta T/(2a(T+T_0)^2) \right)^{1/2}$ and $\mu = \eta$. If $T/(T+T_0)^2$ is assumed to be independent of viscosity [15], we find a relation between driving force and impedance: $f \propto \mu^{1/2}$ (see Table I).

For both active and capillary suction we find that $f \propto \mu^{1/2}$ (i.e. $\gamma = 1/2$) and the optimal concentration $\bar{c}_{opt}$ can therefore be found by maximizing $c/\mu^{1/2}$. For nectar sugar solutions, we therefore predict that $\bar{c}_{opt} = 35\%$ wt/wt and $\mu(\bar{c}_{opt}) = 4\mu_0$ (i.e. $\alpha = 2$ in (7)). This is in good agreement with experimental data on 16 butterfly and hummingbird species (see Fig. 1(a) and Table II), where optimal concentrations in the range $30\% - 45\%$ are reported.

B. Blood flow in vertebrates

Another biological flow problem that can be analyzed within our framework is oxygen and nutrient transport within the cardiovascular system of vertebrate animals. Here, red blood cells transport oxygen between the lungs and distal parts of the organism. The cells are suspended in blood plasma, which primarily consists of water [16]. Red blood cells typically measure 10 μm in diameter [17], and the blood's bulk viscosity increases with the hematocrit $\tilde{c}$, the volume concentration of red blood cells (see Appendix B). While blood with the highest hematocrit is the most oxygen rich, the increase of viscosity with the hematocrit also makes such blood the most difficult to transport. Accordingly, an optimal hematocrit may be sought for maximizing oxygen transport.

In the limit of low Reynolds number Hagen-Poiseuille flow, the red blood cell volume flow rate J_r in vessels larger than 1 mm can be expressed as

$$J_r = \tilde{c} \frac{\pi a^4}{8\eta(\bar{c})l} \Delta p \tag{10}$$

where a and l are the radius and length of the blood vessel, η the blood viscosity (see Appendix B), and Δp the pressure difference generated by the heart. The diastolic pressure is of the order of 10 kPa for most animals [18], but the pressure difference associated with flow in large vessels is small; most of the pressure drop in blood flow occurs in vessels with size comparable to red blood cells. The dependence of blood pressure on the hematocrit is, however, negligible [4], i.e. Δp does not depend on $\tilde{c}$. Although blood viscosity η generally depends on the shear rate, this dependence is weak for typical blood conditions, specifically in vessels with diameters larger than 1 mm and shear rates greater than 50 s^{-1} [16]. Comparing

the blood flow rate in Eq. (10) to the general expression in Eq. (2) we find that $c = \tilde{c}$, $\mu = \eta$, $X = \pi a^4/(8l)$ and $f = \Delta p$. We express the constraint as that of constant pressure $f = f_0 = \Delta p$ (see Table I).

For blood flow we thus find that $Xf \propto \mu^0$ (i.e. $\gamma = 0$) and the optimum concentration $\tilde{c}_{\text{opt}}$ can be found by maximizing c/μ. We therefore predict that $\tilde{c}_{\text{opt}} = 39\,\%$ vol/vol and $\mu(\tilde{c}_{\text{opt}}) = 2\mu_0$ (i.e. $\alpha = 1$, in (7)), in good agreement with experimental data from 57 species observed throughout the animal kingdom (see Fig. 1(b) and Table II). We attribute the significant variation in the observed concentrations in part to the complex interactions between red blood cells and flow in smaller vessels, which we do not consider in our model. An important feature of the red blood cell volume flow rate J_r is also that it varies by less than $20\,\%$ over the range of concentrations from $c = 20\,\%$ to $c = 60\,\%$, suggesting that concentrations in this interval are acceptable given additional biological constraints. For example, also note that for some diving mammals (e.g. Weddell seals and whales), oxygen storage in the blood may also be an important factor, resulting in a higher hematocrit (up to $63\,\%$) [4]. It is also likely that lack of thermoregulation may explain why poikilothermic animals (e.g. the rainbow trout) has a lower hematocrit value ($23\,\%$) than the average, likely due to thermally induced variations in blood viscosity [19].

C. Sugar transport in plants

Plants, like animals, rely on vascular systems for distribution of energy and nutrients. Energy distribution in plants takes place in the phloem vascular system. Here, an aqueous solution of sugars, amino acids, proteins, ions, and signaling molecules flows through a series of narrow elongated cylindrical cells, known as sieve tube elements, that lie end-to-end forming a microfluidic distribution system spanning the entire length of the plant. The flow is driven by differences in chemical potential between distal parts of the plant [20]. While phloem sap with high sugar concentration has the greatest potential for energy transfer, the increase of viscosity with sugar concentration makes it the most difficult to transport. Accordingly, an optimal concentration may again be sought for maximizing energy flow.

Assuming low Reynolds number Hagen-Poiseuille flow, the phloem sugar mass flow rate J_p can be expressed as

$$J_p = \rho \bar{c} \frac{\pi a^4}{8\eta(\bar{c})l} \Delta p \tag{11}$$

where a is the radius of the phloem sieve tube ($a \simeq 10\,\mu\text{m}$), l the length of the plant, $\bar{c}$ the sugar concentration, η the phloem sap viscosity, and Δp the pressure difference driving the flow. By comparing the sugar flow rate (11) to the general expression in (2), we find that $\mu = \eta$, $c = \bar{c}\rho$, $X = \pi a^4/(8l)$ and $f = \Delta p$. We express

the constraint as that of constant pressure $f = f_0 = \Delta p$ (see Table I).

For sugar transport in plants we thus find that $Xf \propto \mu^0$ (i.e. $\gamma = 0$) and the optimum concentration $\bar{c}_{\text{opt}}$ can therefore be found by maximizing c/μ. We find that $\bar{c}_{\text{opt}} = 24\,\%$ wt/wt and $\mu(\bar{c}_{\text{opt}}) = 2\mu_0$ (i.e. $\alpha = 1$, in (7)), in good agreement with experimental data (see Fig. 1(c) and Table II). While sugar concentrations observed in plants generally span a wide range, this analysis provides a rational for the observation that plants that use active sugar loading (data shown in Fig. 1(c)) typically have higher sugar concentration than plants that use passive loading [13]. Active loaders expend metabolic energy to increase the sugar concentration in the phloem [21]. The process is driven by membrane transporters and sugar polymerization and occurs against a sugar concentration gradient. However, in passive loading species, sugars move into the phloem without the use of metabolic energy by traveling down a concentration gradient from sites of carbohydrate synthesis and/or storage to the phloem [13]. We also note that plants with the highest sugar concentrations are crop plants, for example potato ($50\,\%$) and maize ($40\,\%$), suggesting that selection for high crop yield tends to lead to increased sugar concentration in the phloem sap [13].

D. Drinking by viscous dipping

So far, we have limited our attention to transport in closed channels. However, it is straightforward to extend the problem to situations where free surfaces are involved. Most bees whose tongues are solid rather than hollow use a drinking style termed "viscous dipping" in which the fluid is entrained by the tongue surface. The average nectar volume entrained can be expressed by $Q \sim 2\pi a e u$, where a is the tongue radius, e the thickness of the nectar layer on the tongue, and u the tongue extraction speed. Based on Landau-Levich-Derjaguin theory when the Reynolds number $Re \ll 1$ and Bond number $Bo \ll 1$, the nectar film thickness is given by $e \sim a Ca^{2/3}$, where $Ca = \eta u/\sigma \ll 1$ is the ratio of viscous to capillary forces [22]. Since the fluid is entrained on the tongue by viscous forces, we define the driving force and geometric factor as $f = \eta u e/a^2$ and $X = 2\pi a^3$. The movement of the tongue in the fluid requires power $W \sim \eta u^2 l$ to overcome the viscous drag, where l is the immersed tongue length. Assuming a constant work rate W for a given creature leads to the constraint on velocity $u \sim (W/(\eta l))^{1/2}$ which leads to $f \propto \mu^{5/6}$ [9] (see Table I).

For viscous dipping, we find that $f \propto \mu^{5/6}$ (i.e. $\gamma = 5/6$) and the optimum concentration $\bar{c}_{\text{opt}}$ can therefore be found by maximizing $c/\mu^{1/6}$. We find that $c_{\text{opt}} = 57\,\%$ wt/wt and $\mu(c_{\text{opt}}) = 64\mu_0$ (i.e. $\alpha = 6$, c.f. Eq. (7)). This is in reasonable agreement with experimental data on 6 bees species (see Fig. 1(d) and Table II), where optimal concentrations in the range $50\,\% - 60\,\%$ are found. This may explain why the nectar concentration of flowers
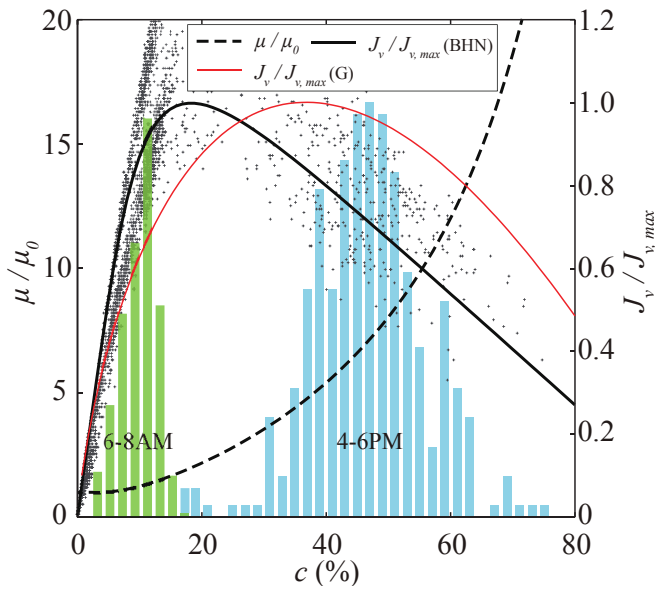
FIG. 2. Optimal vehicle concentration for maximizing traffic flow. Grey dots show measured vehicle flow rate J_v plotted as a function of vehicle concentration $c = \rho/\rho_{opt}$ where $\rho_{opt} = 133$ vehicles/km. The flow rate is normalized by 1483 vehicles/hour which corresponds to $J_v(\rho_{opt}) = J_{v,max}$ in Bando, Hasebe, and Nakayama's (BHN) model [23]. Histograms show the states occupied by the system in the morning (green, 6-8AM) and evening (blue, 4-6PM) rush-hour traffic. The data were collected by the Minnesota Department of Transportation from a sensor on the westbound direction of I-94 (Minneapolis, MN, USA) on Fridays (7, 14, 21, 28) in September 2012 [24]. The predicted vehicle transport rate $J_v/J_{v,max}$ (thick solid black line: BHN model; thin solid red line: Greenberg's model) and traffic impedance μ/μ_0 (dashed line: BHN model) are plotted as a function of vehicle concentration c. The experimental data are available in the Electronic Supplementary Material.

pollinated by bees is generally higher than that of those pollinated by tube feeding butterflies and hummingbirds [9].

IV. APPLICATIONS TO ENGINEERED TRANSPORT SYSTEMS: TRAFFIC FLOW

We have thus far seen many qualitative similarities between different biological flows. Although the detailed physiological and physical mechanisms are different, provided increased concentration leads to greater impedance, we can rationalize the optimal concentrations. An interesting question naturally arises. In which engineered systems might one expect to observe similar phenomena? It appears likely that most efficient communication and transport systems will exhibit similar features. Nevertheless, we limit our discussion to traffic congestion on highways.

A measure of the efficiency of a given section of road is the vehicle flow J_v, the number of vehicles passing a given point per unit time [25–28]. Designers of road networks strive to maximize the vehicle flow which can be expressed as $J_v = \rho v$, where v is the speed of the individual vehicle and ρ the number of vehicles per unit length of roadway. Generally, car speed $v = v(\rho)$ is a decreasing function of density ρ. At very low densities, where inter-vehicle interaction is negligible, however, the speed approaches the speed limit v_{max} and the vehicle flux is proportional to density $J_v \simeq \rho v_{max}$. At higher vehicle densities, interaction between adjacent cars leads to flow impedance and a significant reduction in the speed of individual vehicles, causing congestion and a net decrease in the flux J_v. The vehicle interactions initially take the form of synchronized flow, a form of congested traffic in which each driver attempts to maintain a safe distance from the neighboring cars. As the density increases, wide moving jams form, that is, stop-and-go traffic in which the vehicle flux approaches zero [25]. From these considerations, one anticipates an optimal vehicle density ρ_{opt} that maximizes the vehicle flux.

To estimate ρ_{opt}, we require $v(\rho)$ which can be found either empirically, or deduced from vehicle interaction models. One of the simplest models that leads to a reasonable expression for $v(\rho)$ was proposed by Greenberg [29], who treated traffic flow as a one-dimensional flow of an ideal compressible gas. He assumed (i) that the local speed is a function of density only $v = v(\rho(x,t))$, (ii) that vehicles are conserved $\partial\rho/\partial t + \partial J_v/\partial x = 0$, (iii) that vehicle flow satisfies the Euler equation $Dv/Dt = -(1/\rho)\partial p/\partial x$, and (iv) that traffic "pressure" is proportional to density $p = \mathcal{C}^2\rho$. This leads to the relation $v(\rho) = \mathcal{C}\ln(\rho_{max}/\rho)$ where ρ_{max} is the density at which traffic stops due to congestion. The vehicle flow rate $J_v = \mathcal{C}\rho\ln(\rho_{max}/\rho)$ is at a maximum when $\rho = \rho_{opt} = \rho_{max}/e$, and the constant $\mathcal{C} = v(\rho_{opt})$ is the vehicle speed at the optimal concentration. Since vehicles typically occupy 7.5 m in a totally congested flow [25], we estimate that $\rho_{max} \simeq 133$ vehicles/km. Greenberg's model overestimates the optimal density, predicting $\rho_{opt} = \rho_{max}/e \sim 50$ vehicles/km, while the true value is known to be ~ 20 vehicles/km. Nevertheless, the vehicle flow rate J_v is qualitatively consistent with empirical traffic data, see Fig. 2. The data is plotted as a function of vehicle concentration $c = \rho/\rho_{max}$ in Fig. 2 along with Greenberg's flow rate J_v, deduced using $\rho_{max} = 133$ vehicles/km.

A shortcoming of Greenberg's theoretical model is that the vehicle speed v diverges when the car density is very low. To ensure that $v(\rho/\rho_{max} \to 0) = v_{max}$ and to account for other aspects of traffic flows, numerous other models have been proposed [23, 25–28]. For example, Bando, Hasebe, and Nakayama (BHN) [23] suggested a traffic model in which the vehicle speed depends on the distance from the car in front, Δx. This leads to $v = v_{max}\tanh(\Delta x/s)$, where s is a fixed length scale determined by the road conditions. With a minimum vehicle distance $L = 7.5$ m, we can express the density in terms of Δx as $\rho = 1/(L + \Delta x)$. This leads to

$v(\rho) = v_{\max} \tanh[(1/\rho - L)/s]$, in which case the flow rate $J_v = v\rho$ is optimized when $\rho = 0.21\rho_{\max} = 28$ vehicles/km. With $v_{\max} = 120$ km/h and $s = 60$ m, the BHN model provides a better quantitative fit to the empirical data than Greenberg's model (see Fig. 2).

Comparing the Greenberg and BHN models of traffic flow to the formulation introduced in Eq. (2), we see that traffic flow can be treated in the same general framework where

$$X = N, \quad f = \mathcal{C} = v(\rho_{\mathrm{opt}}), \quad \mu = (\ln \rho_{\max}/\rho)^{-1} \quad (12)$$

for Greenbergs model, and

$$X = N, \quad f = v_{\max}, \quad \mu = \tanh\left(\frac{1 - \rho L}{\rho s}\right)^{-1} \quad (13)$$

for the BHN model. In both cases, N is the number of lanes.

Comparing traffic flow to the biological transport problems considered above, we find that the normalized flux and impedance curves follow the same pattern (see Fig. 2). While traffic flow can be treated in the same framework as biological flows, it is important to note that the congested highway (Fig. 2, data recorded from 4-6 PM) is very far from being optimized. This is presumably due to two main effects. First, the individual vehicle operator attempts to minimize his or her own travel time which does not necessarily optimize the overall vehicle flow J_v. Second, traffic flows are intrinsically time dependent which leads to the formation of traveling density waves and shocks [25–28].

V. UNIVERSAL PROPERTIES OF TRANSPORT SYSTEMS

To compare characteristics of the particular biological and man-made transport systems considered in Sec. III and IV to the general formulation in Eqns. (4) and (6), normalized material flow and impedance curces are plotted in Fig. 3. Despite the complex dependence of impedance on concentration (see Appendices A and B), both the material flow J^* and impedance μ^* are adequately approximated by the simple forms given in Eqns. (4) and (6). From (6), it follows that the impedance at the optimum concentration is $\mu_{\mathrm{opt}} = 2^\alpha \mu_0$, where μ_0 is the impedance of the pure carrier medium (with $c = 0$) and the power α is determined by the flow constraints. In the cases of vascular transport in plants and animals, the power $\alpha = 1$, since there is no coupling between the constant driving pressure (f) or the vascular geometry (X) and the impedance (μ). This suggests that the optimum in material flow should occur when the blood or phloem sap is twice as viscous as water, i.e. $\eta_{\mathrm{opt}} = 2\eta_0$, in good agreement with observed values (see Table II).

In transport systems that are constrained, for example by constant work rate, α will generally be greater

TABLE II. Comparison between theoretical predictions (T) and experimental observations (E) of the optimum concentration c_{opt}, the optimum viscosity μ_{opt} and the exponent α. Concentration units are % wt/wt for nectar drinking and sugar transport in plants, % vol/vol for blood flow, and % vehicle density/max vehicle density for traffic flow. The experimental data are available in the Electronic Supplementary Material.

System	c_{opt}		μ_{opt}/μ_0		α	
	T	E	T	E	T	E
Nectar drinking (Suction)	35	36.9 ± 5.3	4	$3.5 - 7.4$	2	$1.8 - 2.9$
Blood flow in vertebrates	39	40.2 ± 8.6	2	$2.2 - 3.4$	1	$1.1 - 1.8$
Sugar transport in plants	24	21.8 ± 10.3	2	$1.4 - 3.6$	1	$0.5 - 1.8$
Nectar drinking (Viscous dipping)	57	55.0 ± 4.1	64	$17.5 - 49.4$	6	$4.1 - 5.6$
Traffic flow (Greenberg)	37	18	-	-	-	-
Traffic flow (BHN)	21	18	2	1.9	1	0.9

than unity, because of the coupling between flow and impedance. The impedance at the optimum concentration $\mu_{\mathrm{opt}} = 2^\alpha \mu_0$, can therefore be significantly greater than that of the carrier medium. This is most clearly seen in the case of viscous dipping (Sec. III D), where the observed nectar viscosity is up to 50 greater than that of water, roughly consistent with the value ($2^6 = 64$) predicted by our simple model (see Table II).

These observations suggest that this general framework may also provide rationale for the viscosities found in other biological transport systems where efficient transport is favored. Examples of systems with constant forcing include mammals that drink whole milk (observed viscosity: $\eta \sim 2\eta_0$ [30]), and in the macro-alga *Chara* where streaming distributes the content of the cell cytosol (observed viscosity: $\sim 3\eta_0$ [31]). Although detailed studies of these systems are left for future consideration, we note that both are roughly consistent with the predictions of our general theory with $\alpha = 1$.

Comparing traffic flow to the biological transport problems considered, we find that the normalized flux and impedance curves follow the same pattern (see Fig. 3 and Table II). Since the speed limit $v_{\max}$, which is fixed on a given road section, corresponds to the flow driving mechanism in the BHN model, traffic flow is analogous to vascular transport in animals and plants that operate at constant pressure. Our model thus indicates that the flow constraint does not couple to impedance, $Xf \propto \mu^0$ ($\gamma = 0$, $\alpha = 1$), and hence that the optimal impedance is $\mu_{\mathrm{opt}} = 2\mu_0$. This is in rough accord with the BHN model which yields $\mu_{\mathrm{opt}} = 1.9\mu_0$.
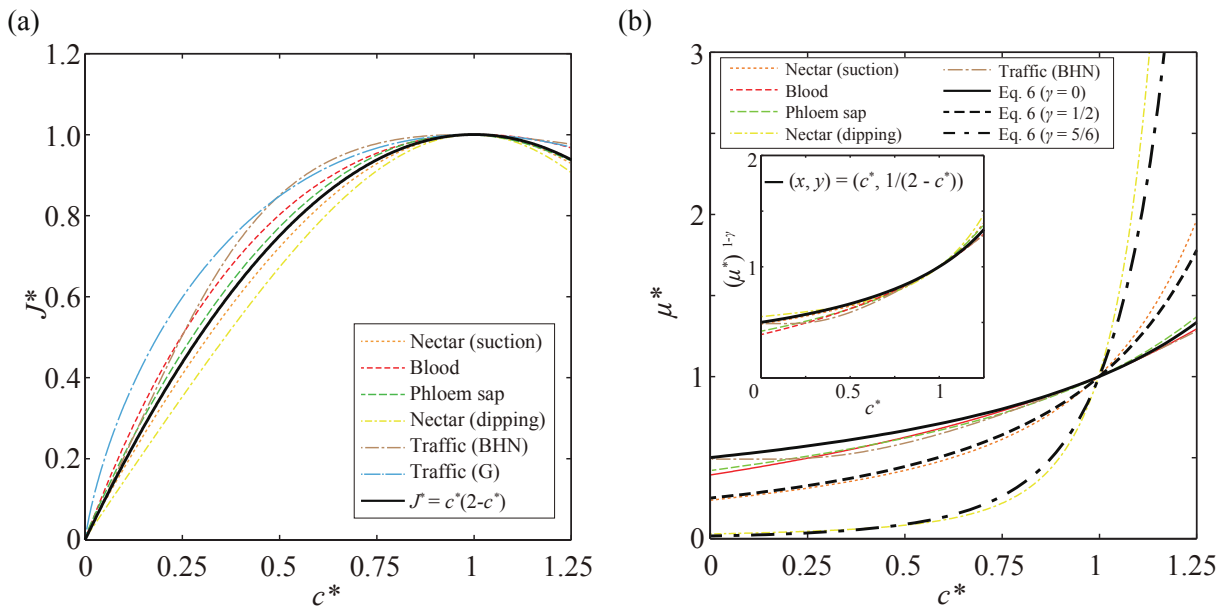
FIG. 3. Universal properties of biological and engineered flows. (a) Normalized flow rate $J^* = J(c)/J(c_{\mathrm{opt}})$ plotted as a function of normalized concentration $c^* = c/c_{\mathrm{opt}}$. The solid thick black line shows the prediction of Eq. (4). (b) Normalized impedance $\mu^* = \mu(c)/\mu(c_{\mathrm{opt}})$ plotted as a function of normalized concentration c^*. The solid and dashed thick black lines show the predictions of Eq. (6). The inset indicates the dependence of $(\mu^*)^{1-\gamma}$ on c^*.

VI. DISCUSSION AND CONCLUSION

We have seen many qualitative and quantitative similarities between different natural and engineered transport systems. Although the detailed mechanisms are different, key common features have allowed us to develop a general framework. Provided impedance increases with concentration, our model provides means of rationalizing the optimal concentrations. Collecting data from more than 100 plant and animal species, we have observed that optimization of material flow appears to be a universal feature of biological transport systems. This deduction provides rational for the observation that the simple model introduced in Sec. II collapses flow and impedance curves for all the systems considered (Fig. 3), suggesting a universal component to all natural transport systems.

Finally, we have shown that an interesting analogy can be made between biological systems and self-driven systems such as traffic flows. Here we find that the impedance analogy is still valid, but that the system is far from optimized due to conflicting interests between individuals and the collective. The consideration of other man-made transport systems, such as the electrical grid or the internet, is left for future consideration.

VII. ACKNOWLEDGEMENTS

Appendix A: Viscosity and density of nectar and phloem sap

Phloem sap and flower nectar consist of an aqueous solution of sugars, amino acids, proteins, and other nutrients. Sugars, of which sucrose, fructose and glucose are the most abundant types, constitute about 90 % of the total solute mass [32]. To approximate the viscosity η and density ρ of phloem sap and nectar, we therefore used data from sucrose solutions of concentration $\bar{c}$ obtained from [12]. Least square fits to sucrose data yields the approximate expressions for viscosity $\eta = \eta_0 g_n(\bar{c}) = \eta_0 \exp\left[0.032\,\bar{c} - (0.012\,\bar{c})^2 + (0.023\,\bar{c})^3\right]$ and density $\rho = \rho_0 \left(1 + 0.0038\bar{c} + (0.0037\,\bar{c})^2 + (0.0033\,\bar{c})^3\right)$. We note that viscosity and density data from other sugar types (glucose and fructose) are well approximated by the fit, suggesting that the major determinant of viscosity is the mass fraction $\bar{c}$, and not the type of solute.

Appendix B: Viscosity of blood

Vertebrate blood is composed of blood cells suspended in blood plasma, a liquid which consists mostly of water. The viscosity of blood η depends primarily on the volume concentration $\tilde{c}$ (hematocrit) of red blood cells, and on

temperature [4, 19]. As demonstrated by Saito [33] and Stark [4], blood viscosity is well described by the function $\eta/\eta_0 = 1 + 2.5\tilde{c}/(1 - \tilde{c})$, which for blood vessels with diameters larger than 1 mm is consistent with empirical data with less than 5% error for $0 < \tilde{c} < 70\%$ [34, 35] (See Table S6 of the Electronic Supplementary Material).

[1] LaBarbera, M. 1990 Principles of design of fluid transport systems in zoology. *Science*, **249**(4972), 992–1000. (doi: 10.1126/science.2396104)

[2] Vogel, S. 2004 Living in a physical world. *Journal of Biosciences*, **29**(4), 391–397.

[3] Murray, C. D. 1926 The physiological principle of minimum work: I. The vascular system and the cost of blood volume. *Proceedings of the National Academy of Sciences of the United States of America*, **12**(3), 207–214.

[4] Stark, H. & Schuster, S. 2012 Comparison of various approaches to calculating the optimal hematocrit in vertebrates. *Journal of Applied Physiology*, **113**(3), 355–67. (doi:10.1152/japplphysiol.00369.2012)

[5] Jensen, K. H., Lee, J., Bohr, T., Bruus, H., Holbrook, N. M. & Zwieniecki, M. A. 2011 Optimality of the Münch mechanism for translocation of sugars in plants. *Journal of the Royal Society Interface*, **8**(61), 1155–1165. (doi: 10.1098/rsif.2010.0578)

[6] Kim, W. & Bush, J. W. M. 2012 Natural drinking strategies. *Journal of Fluid Mechanics*, **705**.

[7] Kim, W., Peaudecerf, F., Baldwin, M. W. & Bush, J. W. M. 2012 The hummingbird's tongue: a self-assembling capillary syphon. *Proceedings of the Royal Society B: Biological Sciences.* (doi: 10.1098/rspb.2012.1837)

[8] Pivnick, K. & McNeil, J. 1985 Effects of nectar concentration on butterfly feeding: measured feeding rates for *Thymelicus lineola* (Lepidoptera: Hesperiidae) and a general feeding model for adult Lepidoptera. *Oecologia*, **66**, 226–237.

[9] Kim, W., Gilet, T. & Bush, J. W. M. 2011 Optimal concentrations in nectar feeding. *Proceedings of the National Academy of Sciences of the United States of America*, **108**(40), 16 618–16 621. (doi:10.1073/pnas.1108642108)

[10] Birchard, G. F. 1997 Optimal Hematocrit: Theory, Regulation and Implications. *Integrative and Comparative Biology*, **37**(1), 65–72. (doi:10.1093/icb/37.1.65)

[11] Nicolson, S. W. 2007 Nectar consumers. In *Nectaries and nectar* (eds S. W. Nicolson, M. Nep & E. Pacinir), pp. 289–342. Dordrecht: Springer-Verlag.

[12] Haynes, W. M. (ed.) 2012 *CRC Handbook of Chemistry and Physics*. Boca Raton, FL: CRC Press, 93rd edn.

[13] Jensen, K. H., Savage, J. A. & Holbrook, N. M. 2013 Optimal concentration for sugar transport in plants. *Submitted to Journal of the Royal Society Interface.*

[14] Kingsolver, J. & Daniel, T. 1983 Mechanical determinants of nectar feeding strategy in hummingbirds: energetics, tongue morphology, and licking behavior. *Oecologia*, **60**, 214–226.

[15] Hainsworth, F. 1973 On the tongue of a hummingbird: its role in the rate and energetics of feeding. *Comparative Biochemistry and Physiology*, **46**, 65–78.

[16] Robertson, A. M., Sequeira, A. & Kameneva, M. V. 2008 *Hemodynamical Flows*, vol. 37 of *Oberwolfach Seminars*. Basel: Birkhäuser Basel. (doi:10.1007/978-3-7643-7806-6)

[17] Gregory, T. 2000 Nucleotypic effects without nuclei: genome size and erythrocyte size in mammals. *Genome*, **901**, 895–901.

[18] Seymour, R. & Blaylock, A. 2000 The principle of laplace and scaling of ventricular wall stress and blood pressure in mammals and birds. *Physiological and Biochemical Zoology*, **73**(4), 389–405.

[19] Eckmann, D. M., Bowers, S., Stecker, M. & Cheung, A. T. 2000 Hematocrit, volume expander, temperature, and shear rate effects on blood viscosity. *Anesthesia & Analgesia*, **91**(3), 539–545.

[20] Jensen, K. H., Liesche, J., Bohr, T. & Schulz, A. 2012 Universality of phloem transport in seed plants. *Plant, Cell and Environment*, **35**(6), 1065–1076. (doi: 10.1111/j.1365-3040.2011.02472.x)

[21] Rennie, E. A. & Turgeon, R. 2009 A comprehensive picture of phloem loading strategies. *Proceedings of the National Academy of Sciences of the United States of America*, **106**(33), 14 162–14 167. (doi: 10.1073/pnas.0902279106)

[22] de Gennes, P.-G., Brochard-Wyart, F. & Quere, D. 2003 *Capillarity and Wetting Phenomena: Drops, Bubbles, Pearls, Waves (Google eBook)*. New York: Springer.

[23] Bando, M., Hasebe, K. & Nakayama, A. 1995 Dynamical model of traffic congestion and numerical simulation. *Physical Review E*, **51**(2), 1035–1042.

[24] Minnesota Department of Transportation, Mn/DOT Traffic Data. Website. http://data.dot.state.mn.us/datatools.

[25] Schadschneider, A. 2002 Traffic flow: a statistical physics point of view. *Physica A: Statistical Mechanics and its Applications*, **313**, 153–187.

[26] Seibold, B., Flynn, M., Kasimov, A. & Rosales, R. 2012 Constructing set-valued fundamental diagrams from jamiton solutions in second order traffic models. *arXiv preprint*, p. 1204.5510.

[27] Helbing, D. 2001 Traffic and related self-driven many-particle systems. *Reviews of modern physics*, **73**(4), 1067–1141.

[28] Flynn, M. R., Kasimov, A. R., Nave, J.-C., Rosales, R. R. & Seibold, B. 2009 Self-sustained nonlinear waves in traffic flow. *Phys. Rev. E*, **79**, 056 113. (doi: 10.1103/PhysRevE.79.056113)

[29] Greenberg, H. 1959 An analysis of traffic flow. *Operations Research*, **7**(1), 79–85.

[30] McCarthy, O. & Singh, H. 2009 Physico-chemical properties of milk. In *Advanced dairy chemistry* (eds P. McSweeney & P. F. Fox), pp. 691–758. Springer New York. (doi:10.1007/978-0-387-84865-5˙15)

[31] Scherp, P. & Hasenstein, K. H. 2007 Anisotropic viscosity of the chara (characeae) rhizoid cytoplasm. *American Journal of Botany*, **94**(12), 1930–1934. (doi: 10.3732/ajb.94.12.1930)

[32] Pate, J. 1976 Nutrients and metabolites of fluids recovered from xylem and phloem: significance in relation to long-distance transport in plants. In *Transport and trans-*

fer processes in plants (eds I. F. Wardlaw & J. B. Passioura), pp. 253–281. New York: Academic Press.

[33] Saitô, N. 1950 Concentration dependence of the viscosity of high polymer solutions. I. *Journal of the Physical Society of Japan*, **5**(1), 4–8. (doi:10.1143/JPSJ.5.4)

[34] Pries, A., Neuhaus, D. & Gaehtgens, P. 1992 Blood viscosity in tube flow: dependence on diameter and hematocrit. *American Journal of Physiology*, **263**, 1770–1778.

[35] Green, H. 1950 Circulatory system: physical principles. *Medical physics*, **2**(228).